ELSEVIER

25 September 2000

Physics Letters A 274 (2000) 228–235

PHYSICS LETTERS A

www.elsevier.nl/locate/pla

Pair distribution functions of dense partially ionized hydrogen

V.S. Filinov [a,1], V.E. Fortov [a], M. Bonitz [b,*], D. Kremp [b]

[a] *Russian Academy of Sciences, High Energy Density Research Center, Izhorskaya street 13–19, Moscow 127412, Russia*
[b] *Fachbereich Physik, Universität Rostock, Universitätsplatz 3, D-18051 Rostock, Germany*

Received 28 June 2000; accepted 3 August 2000
Communicated by V.M. Agranovich

Abstract

Using a novel path integral representation of the many-particle density operator, we calculate the pair distribution function of Fermi systems which are both *strongly coupled and strongly degenerate*. Numerical results are presented for a dense two-component electron–proton plasma at temperatures $k_B T > 0.1$ Ry.

PACS: 52.25.Ub; 52.65; 31.15.K
Keywords: Dense plasmas; Hydrogen; Partial ionized plasma; Path integral Monte Carlo; Pair distribution function

There is growing interest in the thermodynamic properties of Fermi systems in many fields, including plasmas, astrophysics, solids and nuclear matter, see Refs. [1–3] for an overview. Among the phenomena of current interest are Fermi liquids, metallic hydrogen, plasma phase transition, bound states etc., which occur in situations where both Coulomb *and* quantum effects are relevant.

A theoretical approach which is well suited to describe this region is the path integral quantum Monte Carlo (PIMC) method. There has been remarkable recent progress in applying these techniques to Fermi systems, see e.g. Refs. [1,2,4–6]. However, these simulations are hampered by the notorious fermion sign problem. To overcome this difficulty, additional assumptions such as the fixed node and restricted path concepts have been introduced [7] which, however, are difficult to verify. Recently, we have presented a new path integral representation for the N-particle density operator [8–10] which avoids these additional approximations and is based on a *direct fermionic path integral Monte Carlo* procedure. Using this concept we computed the pressure and energy of a degenerate strongly coupled electron–proton plasma in broad range of densities and temperatures, $k_B T > 0.1$ Ry, [8–10]. Further, this method was successfully applied to Wigner crystallization of few-electron systems in traps [11].

In this work we apply our PIMC method to the computation of the pair distribution functions. As an illustration, we present numerical results (i) for an ideal electron–proton plasma which are compared to analytical predictions, (ii) for a nonideal plasma over a wide range of coupling and degeneracy and (iii) investigate the formation of hydrogen atoms and

* Corresponding author. Phone/Fax: (+49)-381-498-1608.
E-mail address: michael.bonitz@physik.uni-rostock.de (M. Bonitz).
[1] Mercator guest professor at Rostock University.

0375-9601/00/$ - see front matter
PII: S0375-9601(00)00554-5

molecules and their vanishing with increased temperature or pressure (Mott effect).

The pair distribution function of a binary mixture of N_e electrons and N_i ions is defined by the density matrix ρ

$$g_{\alpha\gamma}(\boldsymbol{R}_1,\boldsymbol{R}_2) = \frac{1}{Z}\sum_{\sigma}\int_V dq\,dr\,\delta(\boldsymbol{R}_1-\boldsymbol{Q}_1^{\alpha}) \times\delta(\boldsymbol{R}_2-\boldsymbol{Q}_2^{\gamma})\,\rho(q,r,\sigma;\beta), \quad (1)$$

where $\beta = 1/k_{\mathrm{B}}T$, and $q\equiv\{\boldsymbol{q}_1,\boldsymbol{q}_2,\ldots,\boldsymbol{q}_{N_i}\}$ comprises the coordinates of the ions, and $\sigma = \{\sigma_1,\ldots,\sigma_{N_e}\}$ and $r\equiv\{\boldsymbol{r}_1,\ldots,\boldsymbol{r}_{N_e}\}$ denote the electron spins and coordinates, respectively. The indices α and γ label the particle species, i.e. $\alpha = e,i$ and $\gamma = e,i$, and the coordinates $\boldsymbol{Q}$ denote one of the following: $\boldsymbol{Q}_{1,2}^{e} = \boldsymbol{r}_{1,2}$ and $\boldsymbol{Q}_{1,2}^{i} = \boldsymbol{q}_{1,2}$. Furthermore, Z is the partition function given by [13]

$$Z(N_e,N_i,V,\beta) = \frac{Q(N_e,N_i,\beta)}{N_e!N_i!},$$

$$\text{with}\quad Q(N_e,N_i,\beta) = \sum_{\sigma}\int_V dq\,dr\,\rho(q,r,\sigma;\beta). \quad (2)$$

The exact density matrix is, for a quantum system, in general, not known but can be constructed using a path integral representation [13],

$$\rho(q,r,\sigma;\beta) = \frac{1}{\lambda_i^{3N_i}\lambda_{\Delta}^{3N_e}}\sum_{P}(\pm1)^{\kappa_P}\int_V dr^{(1)}\cdots dr^{(n)} \times\rho(q,r,r^{(1)};\Delta\beta)\cdots\rho(q,r^{(n)},\hat{P}r^{(n+1)};\Delta\beta) \times\mathscr{S}(\sigma,\hat{P}\sigma'), \quad (3)$$

where $\Delta\beta\equiv\beta/(n+1)$ and $\lambda_{\Delta}^2 = 2\pi\hbar^2\Delta\beta/m_e$. Further, $r^{(n+1)}\equiv r$ and $\sigma' = \sigma$, i.e. the electrons are represented by fermionic loops with the coordinates (beads) $[r]\equiv[r,r^{(1)},\ldots,r^{(n)},r]$. The electron spin gives rise to the spin part of the density matrix $\mathscr{S}$, whereas exchange effects are accounted for by the permutation operator $\hat{P}$ and the sum over the permutations with parity κ_P. In the fermionic case (minus sign), the sum contains $N_e!/2$ positive and negative terms leading to the notorious sign problem.

Following Refs. [4,8–10], we use a modified representation of the high-temperature density matrices on the r.h.s. of Eq. (3) which is suitable for efficient direct fermionic PIMC simulations of plasmas [14,15]:

$$\sum_{\sigma}\rho(q,r,\sigma;\beta) = \frac{1}{\lambda_i^{3N_i}\lambda_{\Delta}^{3N_e}}\sum_{s=0}^{N_e}\rho_s(q,[r],\beta),$$

$$\rho_s(q,[r],\beta) = \frac{C_{N_e}^{s}}{2^{N_e}}\,e^{-\beta U(q,[r],\beta)}\prod_{l=1}^{n}\prod_{p=1}^{N_e}\phi_{pp}^{l}\det|\psi_{ab}^{n,1}|_s,$$

$$U(q,[r],\beta) = U^{i}(q) + \sum_{l=0}^{n}\frac{U_l^{e}([r],\beta) + U_l^{ei}(q,[r],\beta)}{n+1}, \quad (4)$$

where U^i, U_l^e and U_l^{ei} denote the sum of the binary interaction potentials Φ^{ab} between ions, electrons at vertex 'l' and electrons (vertex 'l') and ions, respectively. The error of thermodynamic quantities computed using Eq. (4) vanishes with growing number of beads at least as $1/(n+1)$ [10]. In Eq. (4), $\phi_{pp}^{l}\equiv\exp[-\pi|\xi_p^{(l)}|^2]$, where we introduced dimensionless distances between neighboring vertices (beads) on the loop, $\xi^{(1)},\ldots,\xi^{(n)}$. Thus, explicitly, $[r]\equiv[r;r+\lambda_{\Delta}\xi^{(1)};r+\lambda_{\Delta}(\xi^{(1)}+\xi^{(2)});\ldots]$. We underline that the density matrix (4) does not contain an explicit sum over the permutations and thus no sum of terms with alternating sign. Instead, the whole exchange problem is contained in a single exchange matrix given by

$$||\psi_{ab}^{n,1}||_s \equiv ||\exp\left\{-\frac{\pi}{\lambda_{\Delta}^2}\left|(r_a-r_{\mathrm{B}})+y_a^{n}\right|^2\right\}||_s, \quad (5)$$

where $y_a^n = \lambda_{\Delta}\sum_{k=1}^{n}\xi_a^{(k)}$. As a result of the spin summation, the matrix carries a subscript s denoting the number of electrons having the same spin projection. For more details, we refer to Refs. [8,9,14,15].

We now explain how to compute the pair distribution function in our scheme. Using the result (4) for

the density matrix, the pair distribution functions (1) become

$$g_{\alpha\gamma}(\boldsymbol{R}_1,\boldsymbol{R}_2) = \frac{1}{\Xi}\int_V dq\,dr\,d\xi\,\delta(\boldsymbol{R}_1-\boldsymbol{Q}_1^{\alpha}) \times\delta(\boldsymbol{R}_2-\boldsymbol{Q}_2^{\gamma})\,\rho(q,[r],\beta), \quad (6)$$

$$\Xi(N_e,N_i,\beta) = \int_V dq\,dr\,d\xi\,\rho(q,[r],\beta). \quad (7)$$

Expression (6) is well suited for numerical evaluation using Monte Carlo techniques, e.g. [4,5]. In our Monte Carlo (MC) scheme we used three types of steps, where either electron or ion coordinates, r_i or q_i or individual electronic beads $\xi_i^{(k)}$ were moved until convergence of the pair distributions was reached. In the simulations we used 50 protons and 50 electrons. To simplify the computations, we included only the dominant contribution in the sum over the total electron spin s corresponding to $s = N/2$ electrons having spin up and down, respectively. (The contribution of the other terms is small and vanishes in the thermodynamic limit.) For the pair potential Φ^{ab} in the high-temperature density matrix we used the Kelbg potential [17][2] which was found to give excellent results for the thermodynamic functions of dense hydrogen [9]. For more details, we refer to Refs. [9,10,14,15].

As a first test, we consider a mixture of *ideal* electrons and protons for which the pair distribution functions are known analytically, see below. Fig. 1 shows our numerical results for the three functions g_{ee}, g_{ii} and g_{ei} as a function of the interparticle distance $\boldsymbol{r} = \boldsymbol{R}_1 - \boldsymbol{R}_2$. As expected, the functions g_{ei} and g_{ii} are identical to one (the fluctuations at small distances reflect the statistical error of the MC simulation, no smoothening has been applied.). In contrast, the electron–electron correlation function decays at small distances reaching 0.5 at $r = 0$ which is the expected result for particles with spin $1/2$.

An interesting feature is the maximum of g_{ee}. It appears around the thermal wavelength λ_e and has a height slightly above 1. At first sight this is surprising as it is in contrast to the familiar analytical result

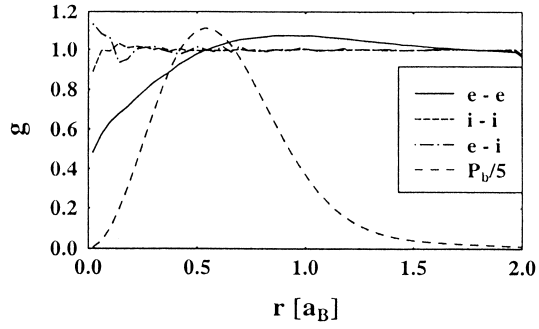

Fig. 1. PIMC result for the pair distribution functions for an *ideal* plasma of degenerate electrons and classical proton at $n\Lambda^3 = 4$.

for the pair distribution function of an ideal Fermi system at zero temperature, e.g. [16],

$$g_0(R) = 1 - \frac{1}{2}\left[\frac{3}{x^3}(\sin x - x\cos x)\right]^2, \quad x = \frac{Rp_F}{\hbar}, \quad (8)$$

where p_F is the Fermi momentum and R the interparticle distance $R_1 - R_2$. Obviously, $g_0 \le 1$ for all R. To find an explanation for the discrepancy between the PIMC result and the behavior of the zero temperature formula (8), we briefly recall the derivation of the analytical result which can be easily extended to finite temperature and even nonequilibrium. Consider the one-particle and two-particle density operators which follow from the N-particle density operator by a partial trace, e.g. [3,19],

$$\hat{F}_1 = V\,\mathrm{Tr}_{2\ldots N}\,\hat{\rho}, \quad \frac{1}{V}\,\mathrm{Tr}_1\,\hat{F}_1 = 1,$$

$$\hat{F}_{12} = V^2\,\mathrm{Tr}_{3\ldots N}\,\hat{\rho}, \quad \frac{1}{V^2}\,\mathrm{Tr}_{12}\,\hat{F}_{12} = 1. \quad (9)$$

Assuming homogeneity, we introduce the momentum representation, with the orthonormal basis functions $|p\sigma\rangle$, with $\sum_\sigma \int d^3p\,|p\sigma\rangle\langle\sigma p| = 1$, and obtain

$$\langle p\sigma|\hat{F}_1|\sigma' p'\rangle = \frac{1}{n} f(p,\sigma)\,\delta(p-p')\,\delta_{\sigma,\sigma'},$$

$$\sum_\sigma \int \frac{d^3p}{(2\pi\hbar)^3} f(p,\sigma) = n. \quad (10)$$

[2] A rigorous justification for the use of the Kelbg potential in PIMC simulations is given in Ref. [18]

For the two-particle density operator of an ideal Bose/Fermi system we obtain

$$\langle p_1\sigma_1 p_2\sigma_2|\hat{F}_{12}|\sigma_2' p_2'\sigma_1' p_1'\rangle = \frac{1}{n^2} f(p_1,\sigma_1) f(p_2,\sigma_2)\{\delta(p_1-p_1') \times\delta(p_2-p_2')\,\delta_{\sigma_1,\sigma_1'}\delta_{\sigma_2,\sigma_2'} \pm \delta(p_1-p_2') \times\delta(p_2-p_1')\,\delta_{\sigma_1,\sigma_2'}\delta_{\sigma_2,\sigma_1'}\}, \tag{11}$$

for arbitrary distribution functions $f(p,\sigma)$. To derive the pair distribution function from Eq. (11) we first compute the two-particle Wigner distribution for the spin diagonal matrix elements, $\sigma_1=\sigma_1'$, $\sigma_2=\sigma_2'$, by Fourier transforming Eq. (11) with respect to the difference momenta $p_1'-p_1$ and $p_2'-p_2$, with the result

$$f_{12}^W(\boldsymbol{p}_1,\boldsymbol{p}_2;\boldsymbol{R};\sigma_1,\sigma_2) = \frac{1}{n^2} f(p_1,\sigma_1) f(p_2,\sigma_2) \times\left\{1\pm\delta_{\sigma_1,\sigma_2} e^{\frac{i}{\hbar}(\boldsymbol{p}_1-\boldsymbol{p}_2)\boldsymbol{R}}\right\}. \tag{12}$$

The pair distribution function is then obtained by summing (12) over σ_1,σ_2 and integrating over p_1,p_2,

$$g(\boldsymbol{R}) = 1\pm\tfrac{1}{2}|\phi(\boldsymbol{R})|^2,$$

$$\phi(\boldsymbol{R}) = \sum_\sigma \int \frac{d^3p}{(2\pi\hbar)^3} f(p,\sigma)\, e^{\frac{i}{\hbar}\boldsymbol{p}\boldsymbol{R}}. \tag{13}$$

This is the pair distribution function of a macroscopic ideal Bose/Fermi gas with an arbitrary distribution function $f(p,\sigma)$. Obviously, for fermions, $g(R)$ is always less or equal unity. If the distribution function is isotropic,

$$\phi(\boldsymbol{R}) \to \phi(R) = \frac{4\pi\hbar}{R}\sum_\sigma \int_0^\infty \frac{dp}{(2\pi\hbar)^3}\, p f(p,\sigma)\sin\frac{pR}{\hbar},$$

and, inserting the zero temperature step function leads immediately to Eq. (8). Inserting Eq. (13) into the normalization condition (9) yields a correction due to the exchange correlations

$$\frac{1}{V^2}\,\mathrm{Tr}_{12}\,\hat{F}_{12} = 1\pm\frac{1}{nN}\sum_\sigma\int\frac{d^3p}{(2\pi\hbar)^3} f^2(p,\sigma), \tag{14}$$

violating the normalization (9). This shows that the result (13) is strictly valid only in the thermodynamic limit where the exchange correction to the normalization vanishes. To reduce the finite size effects, we therefore, performed simulations with increasing particle number and indeed observed a decrease and broadening of the peak.

Let us now turn to the case of *interacting* electrons and protons. Notice that to obtain converging results for the pair distribution functions, requires significantly larger computer time than for the thermodynamic functions. This time increases rapidly with improved spatial resolution of the pair distributions. Therefore, a compromise is necessary, and fluctuations of the pair distributions are unavoidable.

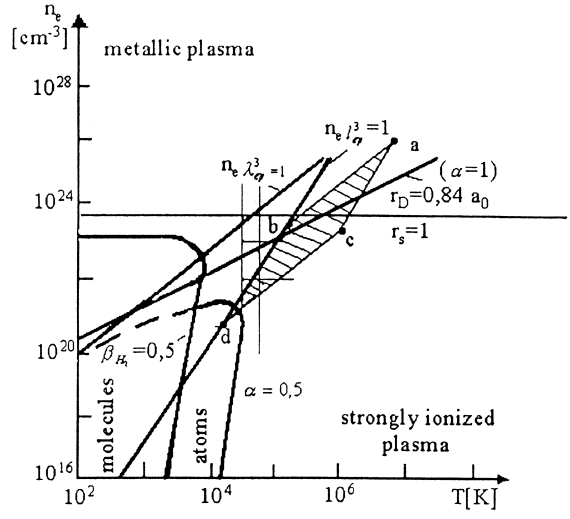

Fig. 2. Qualitative picture of the density-temperature plane of partially ionized hydrogen (from Ref. [20]). Calculations were performed inside the dashed area and along the adjacent vertical and horizontal lines. In particular, dots a–d indicate the simulations points of Fig. 3. Parameters r_D, a_0, r_s, l_{ep}, and λ_{ep} denote the Debye radius, Bohr radius, Brueckner parameter, Landau length and thermal wavelength, respectively. α and β denote the degree of ionization and dissociation respectively, cf. [20].

By performing a series of calculations with varying spatial resolution and bead numbers we determined the optimal parameters. In particular, we found that for temperatures above 0.1 Rydberg it is sufficient to use $n = 6$ beads. As another test, we compared our thermodynamic results to that of recent restricted PIMC simulations [21] and found very good agreement in this temperature range [22].

Let us now discuss the results for a nonideal hydrogen plasma. In contrast to the ideal case, due to Coulomb repulsion, at small distances g_{ee} and g_{ii} decay to zero. However, the decay of g_{ee} is essentially different from that of the proton-proton function due to quantum exchange and tunneling effects in the electron subsystem which compete with the Coulomb repulsion. We have performed a series of calculations over a wide range of values of the classical coupling parameter $\Gamma = (4\pi n_e/3)^{1/3} e^2/4\pi\epsilon_0 kT$ and degeneracy $\chi = n\lambda^3$, for temperatures $T \geq 10{,}000$ K, which is indicated in Fig. 2. In particular, we performed detailed calculations inside the shaded area and along various isotherms and isochors. The most interesting situations are presented below in Figs. 3, 4 and 5. For example, the points a–d refer to qualitatively different physical situations, the corresponding results for the pair distribution functions are presented in Fig. 3. Fig. 3a corresponds to the case of weak coupling and strong degeneracy where both density and temperature are very high. Next, in Fig. 3b, both coupling and degeneracy are strong, whereas Fig. 3c corresponds to weak coupling and weak degeneracy (high temperature). Finally, Fig. 3d shows the pair distribution functions for strong coupling and weak degeneracy (comparatively low temperature and low density). Here, we observe distinct peaks of the electron–elec-

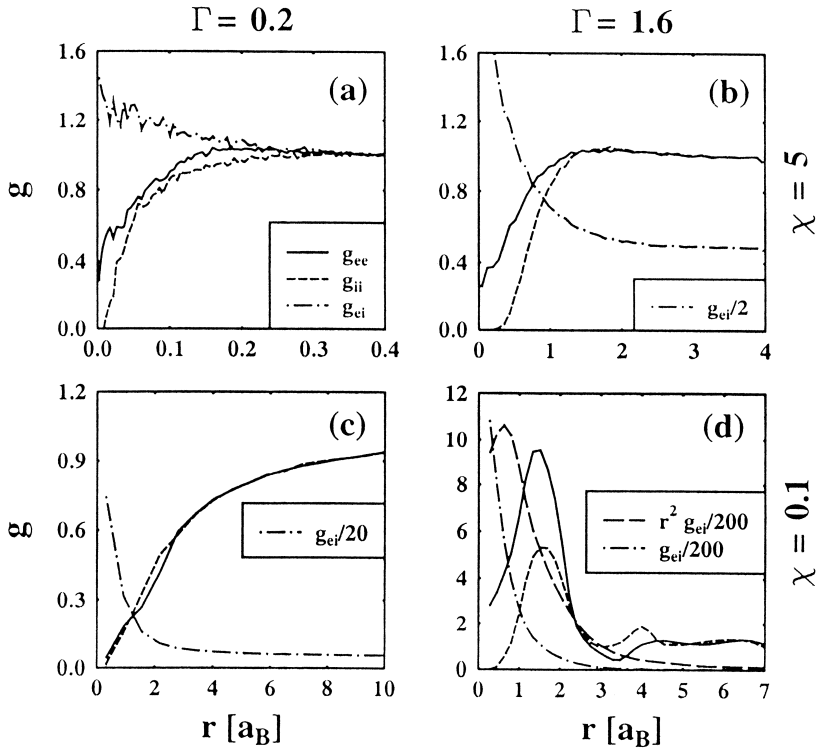

Fig. 3. Pair distribution functions for an electron–proton plasma for four combinations of the coupling and degeneracy parameters Γ and χ. Figure parts (a)–(d) correspond to the points a–d in Fig. 2. (the values are given adjacent to the figures). The corresponding densities and temperatures are (a) $T = 60.5$ Ry, $n = 3.57 \cdot 10^{26}$ cm^{-3}, (b) $T = 0.94$ Ry, $n = 7 \cdot 10^{23}$ cm^{-3}, (c) $T = 4.5$ Ry, $n = 1.43 \cdot 10^{23}$ cm^{-3} and (d) $T = 0.07$ Ry, $n = 2.8 \cdot 10^{20}$ cm^{-3}. Lines styles are shown in inset of (a). Notice the varying length scales and varying scaling of the electron–ion functions.

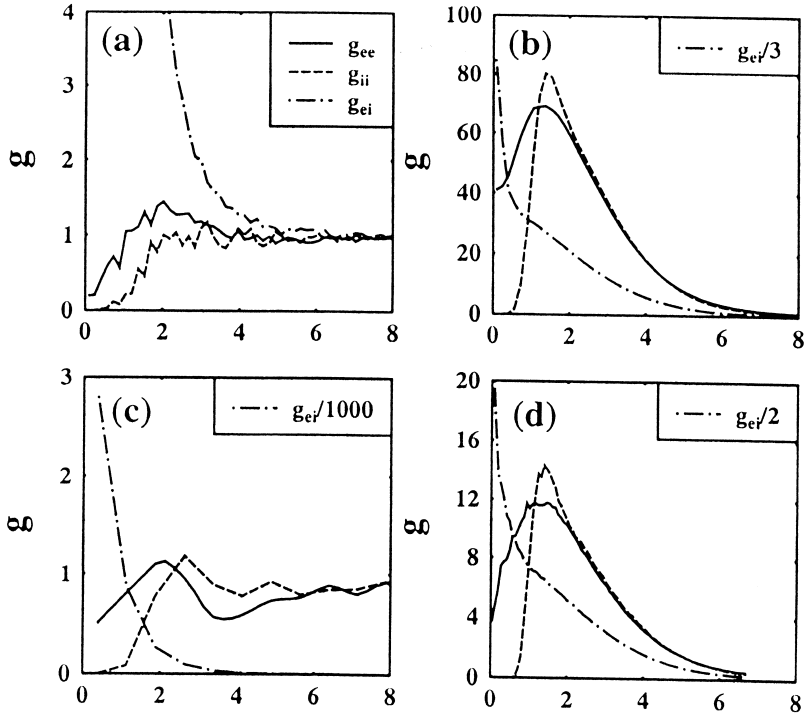

Fig. 4. Electron–electron, ion–ion and electron–ion pair distribution functions of a correlated hydrogen plasma for two temperatures and various densities: (a) $T = 50{,}000$ K, $n = 10^{22}$ cm^{-3}, (b) $T = 20{,}000$ K, $n = 10^{22}$ cm^{-3}, (c) $T = 20{,}000$ K, $n = 10^{20}$ cm^{-3} and (d) $T = 20{,}000$ K, $n = 10^{23}$ cm^{-3}.

tron and ion–ion functions, close to $r = 1.4\,a_B$, clearly indicating the formation of H_2-molecules. The strong peak of g_{ei} (notice the scaling) is caused by hydrogen atoms which is confirmed by considering $r^2 g_{ei}(r)$ which is peaked close to $1\,a_B$. On the other hand, in cases a-c, no distinct peaks of g_{ee}, g_{ii} and $r^2 g_{ei}$ are observed and thus no bound states exist, which is a consequence of high temperature or/and high density.

To analyze the formation of bound states more in detail, in Figs. 4 and 5 we present additional results for lower temperatures. In Fig. 4a and 4b, the pair distribution functions for $n = 10^{22}$ cm^{-3} and $T =$ 50,000 K and $T = 20{,}000$ K, respectively are shown. Obviously, at this density, reduction of the temperature leads to strong enhancement of molecule formation (compare the peak heights). Finally, Figs. 4b–d show the density dependence for a constant temperature $T = 20{,}000$ K, starting from relatively low density, $n = 10^{20}$ cm^{-3}, in Fig. 4c up to high density, $n = 10^{23}$ cm^{-3}, in Fig. 4d. Clearly, the molecular peak grows from c to b which is a result of recombination of hydrogen atoms the fraction of which decreases with increasing density (see Fig. 5 below). Notice that the molecule peak decreases again from b to d which is due to many-body effects (pressure dissociation). The latter cause a reduction of the effective molecule binding energy which eventually leads to pressure dissociation. Notice that at these temperatures, molecules and atoms are co-existing.

We, therefore, investigate the formation of hydrogen atoms at $T = 20{,}000$ K separately in Fig. 5, varying the density over 6 orders of magnitude. Clearly, the highest peak of $r^2 g_{ei}$ is observed for $n = 10^{19}$ cm^{-3}, and it decreases steadily. First, at densities $n \le 10^{22}$ cm^{-3}, this decrease is due to recombination into molecules (cf. Fig. 4). At still higher densities, the atomic fraction is reduced further due to many-body effects (pressure ionization). Interestingly, for densities above $n = 10^{21}$ cm^{-3}, the atomic peak of $r^2 g_{ei}$ shifts from approximately $1\,a_B$ to about $3\,a_B$. This arises from a variety of effects,

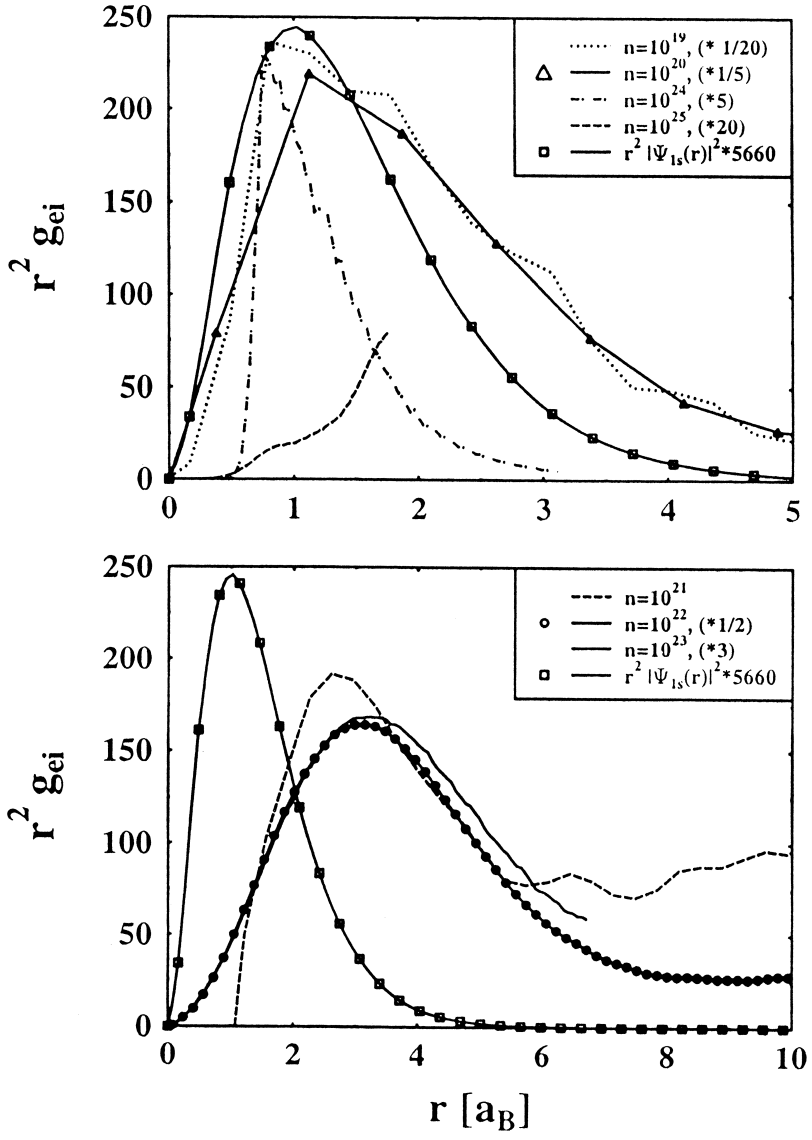

Fig. 5. Electron–ion pair distribution function times r^2 for a correlated electron–proton plasma at $T = 20{,}000$ K for various densities (see inset). Squares denote the shape of the ground state wave function of an isolated hydrogen atom.

but predominantly from the increased molecule fraction, cf. Figs. 4b–d, which favor a broad peak of $r^2 g_{ei}$ in the range from $r \approx a_B$ to $r \approx 3a_B$. Finally, at $n = 10^{24}$ cm^{-3}, the molecules have vanished, and the electron–ion function again shrinks and its peak returns to $r \approx 1a_B$. This density is close to the Mott density (approximately given by $r_D \approx a_B$, cf. Fig. 2). Correspondingly, the height of the peak is strongly reduced, and a further increase to $n = 10^{25}$ cm^{-3} destroys the remaining atoms completely. Finally, it is interesting to compare the shape of the peak of $r^2 g_{ei}$ to that of the hydrogen ground state wave function (squares in Fig. 5). While at low densities the simulations peaks are broader indicating the population of excited states and molecules, at high densities, around $n = 10^{24}$ cm^{-3}, we observe that the

maximum is significantly narrower than the ground state peak.

In summary, we presented results for the pair distribution functions of a correlated quantum plasma using a modified path integral representation (4) for the *N*-particle density matrix. This representation allows one to avoid additional assumptions for the density matrix and to perform efficient direct fermionic simulations for temperatures above approximately 0.1 Ry. Of special interest is the possibility to compute the pair distribution functions for dense partially ionized hydrogen. Our results show that both the formation of atoms and molecules can be well investigated within our scheme. In particular, many-body effects on the bound states, modification of the binding energy, pressure ionization and dissociation are fully included. Further investigations will focus on quantitative estimates for the bound state fraction and a more precise analysis of the Mott transition.

Acknowledgements

We acknowledge support from the Deutsche Forschungsgemeinschaft (Mercator-Programm) for VSF and stimulating discussions with W. Ebeling, W.D. Kraeft and M. Schlanges.

References

[1] Strongly Coupled Coulomb Systems, G. Kalman (Ed.), Pergamon Press 1998.
[2] W.D. Kraeft, M. Schlanges (Eds.), Proc. International Conference on Strongly Coupled Plasmas, World Scientific, Singapore 1996.
[3] W.D. Kraeft, D. Kremp, W. Ebeling, G. Röpke, Quantum Statistics of Charged Particle Systems, Akademie-Verlag, Berlin, 1986.
[4] V.M. Zamalin, G.E. Norman, V.S. Filinov, The Monte Carlo Method in Statistical Thermodynamics, Nauka, Moscow 1977 (in Russian).
[5] K. Binder, G. Ciccotti (Eds.), The Monte Carlo and Molecular Dynamics of Condensed Matter Systems, SIF, Bologna 1996.
[6] B.J. Berne, G. Ciccotti, D.F. Coker (Eds.), Classical and Quantum Dynamics of Condensed Phase Simulation, World Scientific, Singapore, 1998.
[7] D.M. Ceperley, in: Ref. [5], pp. 447–482.
[8] V.S. Filinov, P.R. Levashov, V.E. Fortov, M. Bonitz, in: Ref. [12], (archive: cond-mat/9912055).
[9] V.S. Filinov, M. Bonitz, (archive: cond-mat/9912049).
[10] V.S. Filinov, M. Bonitz, submitted to Eur. J. Phys.
[11] A.V. Filinov, Yu.E. Lozovik, M. Bonitz, Phys. Stat. Sol. (b), accepted for publication (September 2000).
[12] M. Bonitz (Ed.), Progress in Nonequlibrium Green's functions, World Scientific, Singapore, 2000.
[13] R.P. Feynman, A.R. Hibbs, Quantum mechanics and path integrals, McGraw-Hill, New York, 1965.
[14] V.S. Filinov, High Temperature 13 (1975) 1065.
[15] V.S. Filinov, High Temperature 14 (1976) 225.
[16] G.D. Mahan, Many Particle Physics, Plenum Press, New York, 1981.
[17] See W. Ebeling, H.J. Hoffmann, G. Kelbg, Beitr. Plasmaphys. 7 (1967) 233, and references therein.
[18] V. Filinov, W. Ebeling, M. Bonitz, to be published.
[19] M. Bonitz, Quantum Kinetic Theory, Teubner, Stuttgart/Leipzig 1998.
[20] W. Ebeling, W.D. Kraeft, D. Kremp, Theory of Bound States and Ionization Equilibrium in Plasmas and Solids, Akademie-Verlag, Berlin, 1976.
[21] B. Militzer, D. Ceperley, submitted to Phys. Rev. Lett.
[22] V.S. Filinov, V.E. Fortov, M. Bonitz, W. Ebeling, to be published.